



Influences of co-sputtered carbon on the electrochemical performance of SiO/C thin film anodes for lithium-ion batteries

Zulai Cao ^a, Baojia Xia ^b, Xiaohua Xie ^{b,*,**}, Jinbao Zhao ^{a,*}

^a Collaborative Innovation Center of Chemistry for Energy Materials, State Key Lab of Physical Chemistry of Solid Surfaces, State–Province Joint Engineering Laboratory of Power Source Technology for New Energy Vehicle, College of Chemistry and Chemical Engineering, Xiamen University, Xiamen, 361005, PR China

^b Shanghai Institute of Microsystem and Information Technology, China Academy of Sciences (CAS), Shanghai, 201800, PR China

ARTICLE INFO

Article history:

Received 19 December 2018

Received in revised form

7 May 2019

Accepted 9 May 2019

Available online 10 May 2019

Keywords:

Magnetron co-sputtering

SiO/C thin film

Anode

Capacity retention

Structural stability

ABSTRACT

Silicon suboxide (SiO_x) is a promising anode material for lithium-ion batteries due to its high theoretical capacity (~2400 mA h g⁻¹) and good cycle performance. However, the volume effect during cycling and the poor intrinsic electronic conductivity restrict its practical application. Since SiO thin films with carbon additive are able to cope with these limitations, we have synthesized SiO/C thin film anodes containing various carbon contents by magnetron co-sputtering. Among the as-deposited electrodes, SiO/C-80 with a thickness of 1.15 μm showed superior electrochemical performance with an initial coulombic efficiency of ~72%, a maximum reversible specific capacity of 1223 mA h g⁻¹ and a capacity retention of 82.0% ± 0.5% after 750 cycles at a current density of 1 A g⁻¹. The co-sputtered carbon is uniformly dispersed inside the film, which enhances the electronic conductivity and enables higher reversible capacity during the initial cycles. Meanwhile, the co-sputtered carbon plays a role in buffering volume change and maintaining electrode structure during further cycling. These results demonstrated that the SiO/C thin film anode has the application prospect as an anode material for lithium-ion batteries.

© 2019 Elsevier Ltd. All rights reserved.

1. Introduction

Lithium-ion batteries (LIBs) have the advantages of high working voltage, no memory effect, long cycle life, etc., and have been widely used as the power sources of consumer electronics and electric vehicles since their commercialization in 1991. To meet the burgeoning demands for wearable electric equipment and micro electric devices, the all-solid-state LIBs with high energy and long cycle life are expected to be continuously developed [1–4]. In the pursuit of improving electrochemical performance, silicon (Si) has attracted widespread attention because of its high theoretical capacity of 3579 mA h g⁻¹ (Li₁₅Si₄), and is considered as a promising next-generation anode material for LIBs. But its practical application has been still restricted due to its huge volume change (>300%) during cycling, inducing a thicker inert solid-electrolyte-interphase (SEI) layer and the pulverization of active particles, which lead to

drastic capacity fading and poor reversibility [5–8]. Furthermore, the ongoing SEI (re)formation leads not only to electrolyte decomposition, but also to loss of active lithium from the lithium inventory. A major reason for capacity fading of silicon anodes in LIB full cells is the loss of active lithium, in which the lithium content is limited by the cathode material [9,10]. Among various approaches to modify an electrode structure, preparing two-dimensional thin film electrode is considered as a promising candidate because of its high convenience and relatively low cost [11–14]. For instance, Maranchi et al. deposited an amorphous silicon film of 250 nm thickness on copper foil [11]. The Si film exhibited a reversible capacity of nearly 3500 mA h g⁻¹ at 0.4 C for 30 cycles. Wang et al. fabricated a Cu nanoneedle-array (NNA) structure by electroless deposition [12]. After silicon deposition (~100 nm thickness), the electrode exhibited an excellent cycling stability of 1141 mA h g⁻¹ after 1950 cycles at 1.5 C. The Si thin film electrodes have better cycle performance, but when the film thickness increases, the drastic capacity fading is inevitable due to the huge volume effect [11]. In order to further improve the cycle performance, protective coating layers are usually introduced into silicon-based thin film anodes [15–17]. Jouybari et al. prepared bilayer silicon/LiPON thin film anodes by magnetron sputtering

* Corresponding author.

** Corresponding author.

E-mail addresses: xiexiaohua@mail.sim.ac.cn (X. Xie), [jhzha@xmu.edu.cn](mailto:jbzha@xmu.edu.cn) (J. Zhao).

[15]. The LiPON coating layer not only isolated the contact between silicon and electrolyte, which reduced the SEI formation, but also mechanically stabilized the Si electrode, slowed down the process of crack formation and growth. Therefore, the coulombic efficiency and the cycling stability of the silicon can be significantly improved. Tong et al. synthesized amorphous silicon/carbon (a-Si/C) multilayer thin films by magnetron sputtering [17]. Among as-deposited samples, the a-Si/C film with a thickness ratio $d_{\text{Si}}:d_{\text{C}} = 5:1$ showed a high reversible capacity of 2000 mA h g^{-1} over 200 cycles at 1 C and a good structure integrity. The carbon intermediate layers could buffer the volume expansion, enhance the electronic conduction pathway of the electrode and prevent the Si from directly contacting with the electrolyte, thus the a-Si/C multilayer electrode showed excellent electrochemical performance.

Alternatively, silicon suboxide (SiO_x) has a theoretical capacity of $\sim 2400 \text{ mA h g}^{-1}$ and lower volume change ($\sim 200\%$) than silicon, and the SiO_x film electrodes with higher areal capacity are more promising for long cycling applications [18–20]. Researchers have proven that SiO_x films have a complex structure consisting nanosized Si core with SiO_x shell embedded in amorphous SiO_2 matrix [18,21,22]. The first lithiation of SiO_x results in the formation of Li-silicates and Li_2O , and these inactive compounds act as a physical buffer to mitigate the volume change in the following cycles, which enable an enhanced cycle stability [23–25]. The previous studies on SiO_x films have mostly focused on the effects of oxygen content on the electrochemical behaviors. Meng et al. prepared SiO_x thin films with various oxygen contents, among which the $\text{SiO}_{0.7}$ had a specific capacity of $463 \mu\text{A h cm}^{-2} \mu\text{m}^{-1}$ and a capacity retention of 90% after 300 cycles at 0.2 C [26]. Hideharu et al. prepared SiO_x thin films with different x values by reactive evaporation [27]. The $\text{SiO}_{1.02}$ with a thickness of $8.9 \mu\text{m}$ had a discharge capacity of 2.3 mA h cm^{-2} , and a capacity retention of 99.8% after 30 cycles. Miyazaki et al. prepared Si-rich suboxide ($\text{SiO}_{0.4}$) film electrode, which exhibited a high capacity over 2800 mA h g^{-1} and faded only 6% after 100 cycles in all-solid-state batteries [20]. Nevertheless, SiO_x has poor electronic conductivity ($\sim 10^{-12} \text{ S cm}^{-1}$), low initial coulombic efficiency and volume effect. When used as anode material, it is often required to be combined with carbon materials to improve its cycle stability [28–30], since the carbon materials have

admirable electronic conductivity and higher structural stability. Notably, the performance of carbon-combined SiO_x film electrodes have not been reported yet.

In this work, we have investigated the influences of carbon content on the electrochemical properties of SiO/C thin film anodes. The anodes have been prepared by magnetron co-sputtering with a SiO target and a carbon target (Fig. 1), which enables a homogeneous dispersion of carbon inside the films. We have analyzed the influences of co-sputtered carbon based on the change of the electrode morphology and structure, as well as the charge transfer and ion diffusion properties during cycling.

2. Experimental

2.1. Preparation of the SiO/C thin film anodes

The SiO/C thin film anodes were synthesized by magnetron sputtering with a SiO target (Shenzhen Canyon, 99.99% purity) and a carbon target (Shenzhen Canyon, 99.99% purity). The films were deposited on two different substrates respectively: copper foils (Huizhou United Copper Foils Electronic Materials Co., Ltd. diameter: 14 mm, thickness: $16 \mu\text{m}$, 99.9% purity) for electrochemical measurements, and Si wafers (Suzhou Crystal Silicon Electronic & Technology Co., Ltd. p-type monocrystalline, $400 \mu\text{m}$ thick) for cross section view. Before sputtering, the substrates were cleaned with ethanol and acetone for 10 min. The targets were pre-sputtered at 150 W for 10 min in order to remove the surface oxides. The chamber vacuum was 10^{-5} Pa and the working pressure was 0.6 Pa. The SiO/C films were deposited on a radio frequency magnetron sputtering apparatus (Shanghai Full-E Vacuum Equipment Co., China). A constant input power of 200 W was applied to the SiO target, and the carbon content was controlled by changing input powers of carbon target to 40, 80, and 120 W. The deposition time was 300 min to ensure the same content of SiO , and the

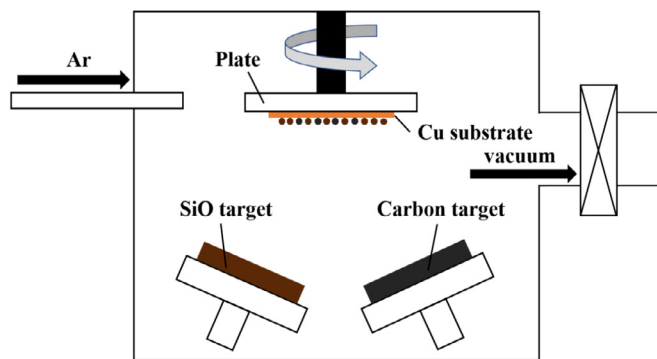


Fig. 1. Schematic illustration of co-sputtering system.

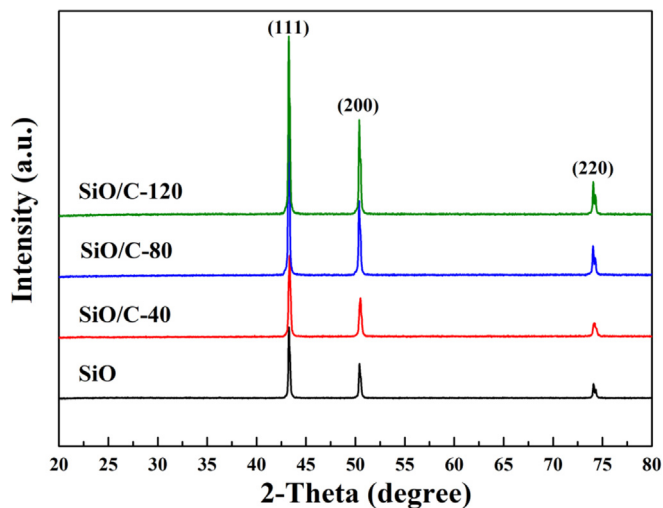


Fig. 2. XRD patterns of as-deposited thin films on Cu substrate.

Table 1

Preparation conditions and components of SiO/C thin films.

Sample	SiO input power (W)	C input power (W)	Deposition time (min)	Thickness (μm)	Atomic ratio (Si: O: C)	Carbon concentration (wt.%)
SiO	200	0	300	~ 1.06	47.3: 52.7	0
$\text{SiO}/\text{C}-40$	200	40	300	~ 1.10	40.6: 44.3: 15.1	8.9
$\text{SiO}/\text{C}-80$	200	80	300	~ 1.15	37.5: 39.8: 22.7	13.9
$\text{SiO}/\text{C}-120$	200	120	300	~ 1.20	35.6: 36.1: 28.3	17.7

samples were labeled as SiO/C-40, SiO/C-80 and SiO/C-120, respectively. SiO film was also deposited with an input power of 200 W for 300 min (Table 1).

2.2. Structural characterizations

X-ray diffraction (XRD, Rigaku D/max 2200, Japan) was used to determine the crystal structures of the as-deposited films. Field emission scanning electron microscopy (FE-SEM, Hitachi S4700, Japan) was used to characterize the surface morphology and film thickness. Energy dispersive X-ray spectrometry (EDS) was used to characterize the distribution of elements inside the as-deposited films. The chemical state of SiO/C films was analyzed by X-ray photoelectron spectroscopy (XPS, Kratos AXIS ULTRA DLD, U.K.) with an Al K α ($h = 1486.7$ eV) radiation. The as-deposited thin films were weighed by an analytical balance with a precision of ± 10 μg (Zanwei, ZA305AS, China). The atomic ratio of Si, O and C, as well as the average concentrations of carbon in the SiO/C films were obtained from the EDS-mapping results.

2.3. Electrochemical characterization

The electrochemical properties were evaluated by CR2025-type

coin cells which were assembled in an argon-filled glovebox. The SiO (or SiO/C) film deposited on Cu foil (diameter: 14 mm) was used as the cathode and a lithium foil (China Energy Lithium Co., Ltd. diameter: 15.6 mm, thickness: 0.45 mm) was used as the anode. The separator was the Celgard 2320 PP/PE/PP film (Celgard Inc., USA), and the electrolyte was 1 M LiPF $_6$ dissolved in ethylene carbonate (EC) and dimethyl carbonate (DMC) (1:1 v/v) containing 5% fluoroethylene carbonate (FEC) (Zhuhai Smoothway Electronic Materials Co., Ltd.). The amount of the electrolyte was 100 μl .

The galvanostatic tests were carried out on Neware battery testing system (Neware, China) at room temperature (298 K), using a current density of 0.05 A g $^{-1}$ for the first cycle, 0.1 A g $^{-1}$ for two cycles as activation process and 1.0 A g $^{-1}$ for the following cycles between 0.01 and 1.5 V. The cyclic voltammetry (CV) and electrochemical impedance spectroscopy (EIS) measurements were carried out with the VSP-300 electrochemical workstation (Bio-Logic, UK). The scan rate was 0.05 mV s $^{-1}$ and the potential window was 0.01–1.5 V (vs. Li/Li $^+$, the same below) for the CV tests. The EIS measurements were carried out with a frequency range from 100 kHz to 0.01 Hz and an amplitude of 10 mV. Three cells were assembled for each material in each electrochemical characterization to ensure a high reproducibility.

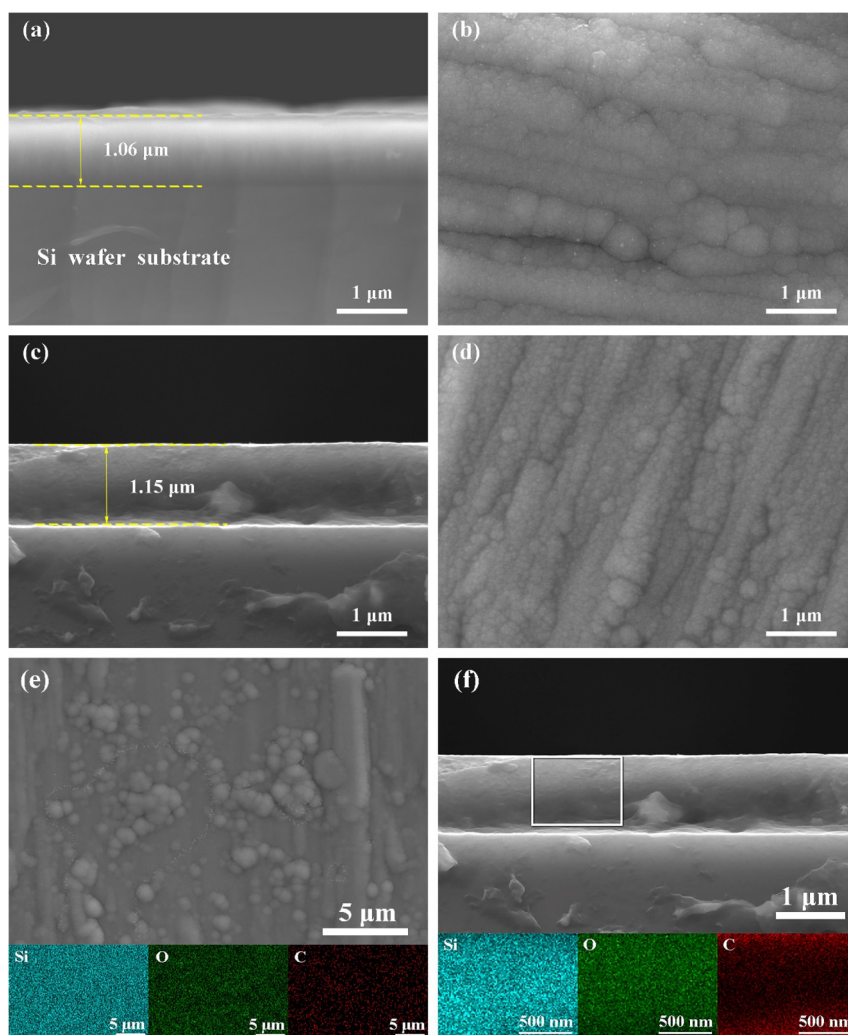


Fig. 3. SEM images of cross section and surface morphology of as-deposited (a) (b) SiO, (c) (d) SiO/C-80. EDS images of (e) the surface morphology and (f) the cross section of as-deposited SiO/C-80 and elemental mapping of Si, O, C.

3. Results and discussion

3.1. Characterization of SiO/C composite film

The XRD patterns of as-deposited SiO/C thin films are shown in Fig. 2. No obvious peaks corresponding to crystalline Si, SiO₂ or C except those of the Cu substrate can be observed in the diffraction patterns. The XRD peaks suggest that the as-deposited SiO/C thin films are amorphous. Since amorphous Si-based materials have no long-range or ordered structure, which show homogeneous volume expansion and contraction during Li insertion and extraction, they may exhibit improved electrochemical performance [8,31].

The surface morphology and film thickness of SiO/C films have been measured by FE-SEM, as shown in Fig. 3. The cross-section SEM images of SiO/C films deposited on the Si wafer show that the as-deposited films are dense, and the film thickness grows with the increase of the carbon target power (Fig. 3). As shown in Fig. 3b and d, SiO and SiO/C films show a rough surface morphology without voids or pinholes, and have a familiar surface morphology like as a SiO film. To further confirm the atomic ratio and distribution of Si, O and C in the films, EDS mapping have been carried out, as shown in Table 1 and Fig. 3e and f. The C distribution is relatively uniform in both surface and depth direction, which can help improve the electronic conductivity inside the SiO thin film.

The XPS spectra of as-deposited SiO/C thin films are shown in Fig. 4. The broad Si 2p peak confirms that the Si exists in different valence states in SiO, which is consistent with the previous work [25,32]. The binding energies of as-deposited SiO/C films are 102.95, 102.90, 102.70 and 102.55 eV, respectively (Fig. 4b). The main peaks of the carbonic samples shift to a lower binding energy, and weak peaks are observed around 99.80 eV in Si 2p spectra, indicating that the Si valence state decreases with the carbon co-

sputtering (Fig. 4b). Similarly, the peaks of the carbonic samples in O 1s spectra also shift to a lower binding energy, and weak peaks are observed around 288.5 eV in C 1s spectra, suggesting that a small amount of carbon reduces Si and combines with O (Fig. 4c and d) [33].

3.2. Electrochemical properties

The electrochemical properties of as-deposited SiO/C thin films during the first lithiation/delithiation process are summarized in the Table 2. The measured lithiation capacity of SiO thin film is 1775 mA h g⁻¹, the delithiation capacity is 1012 mA h g⁻¹, and the initial coulombic efficiency (ICE) is ~57.0%. The low ICE is attributed to the irreversible conversion reaction. On the other hand, since SiO film suffers from a poor electronic conductivity, the lithium in the Li–Si alloy may not be completely extracted. With the carbon co-sputtering, the first delithiation capacity as well as the ICE of SiO/C-40 and SiO/C-80 are significantly improved, but those of SiO/C-120 decreased (Table 2). Previous study on SiO thin film has suggested that at the beginning of the first lithiation process, the main reactions are the formation of inert Li₂O and Li silicates [34], which corresponds to a plateau on the lithiation curves (Fig. 5a). It is found that the plateau voltage of SiO is around 0.22 V and increases with the carbon addition. SiO/C-80 exhibits a highest plateau voltage of 0.42 V among the as-deposited electrodes, suggesting that it has the lowest polarization during the first lithiation process. The plateau voltage of SiO/C-120 is found to be higher than SiO but lower than SiO/C-40 and SiO/C-80, indicating that an excessive amount of carbon may increase the reaction polarization, thus generating a negative impact on the electrochemical properties of the electrode. Since the delithiation reaction of silicon is a process where the internal resistance of the electrode increases [35], for the

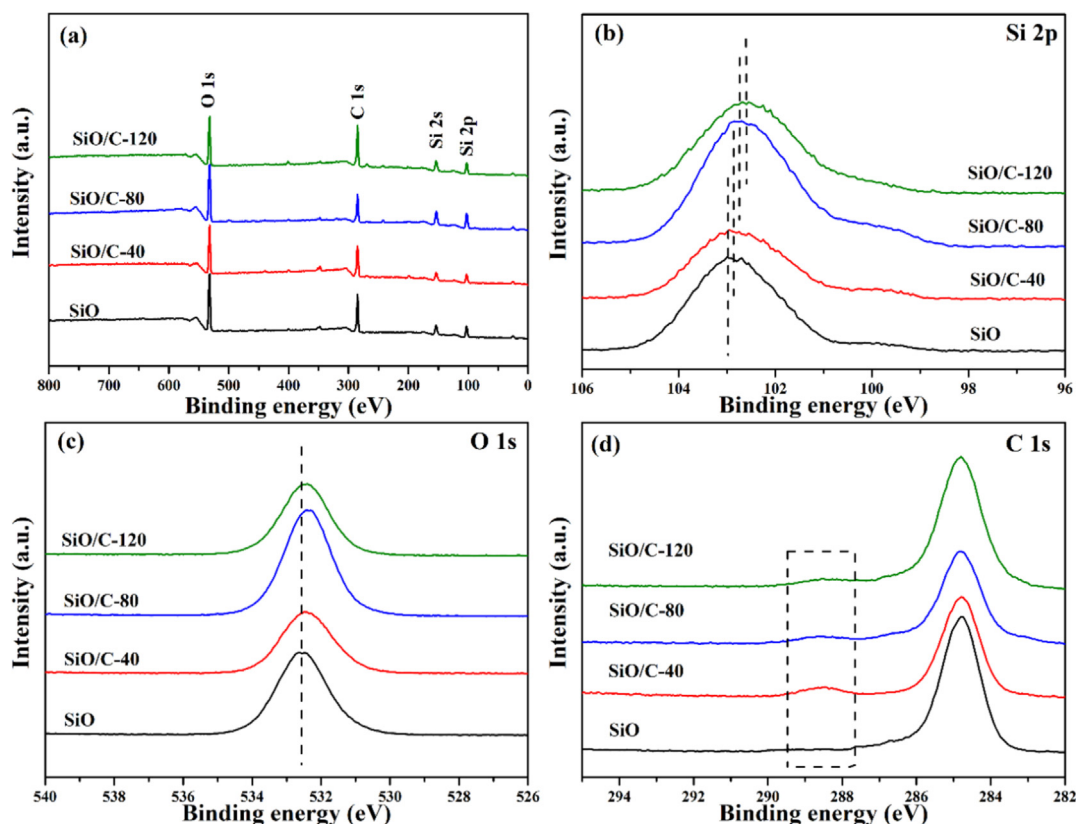


Fig. 4. XPS spectra of (a) full spectra (b) Si 2p (c) O 1s and (d) C 1s of as-deposited SiO/C thin films.

as-deposited SiO, the capacity at the end of the first delithiation process (Fig. 5a, above 0.75 V) accounts for a small part of the total capacity, and some of the lithium in the Li–Si alloy cannot be extracted due to kinetic factors. The co-sputtered carbon will multiply the electronic conductivity inside the SiO film, which is beneficial to extract more lithium at the end of the delithiation process, thus the delithiation capacity and the ICE increase. However, for SiO/C-120, although it has better electronic conductivity than SiO, we speculate that excessive co-sputtered carbon is similar to a successive graphene coating layer, which has a steric hindrance to lithium ion diffusion [36], thus the capacity and the ICE are lower than SiO/C-40 and SiO/C-80.

Fig. 5b shows the average delithiation capacity of as-deposited SiO/C films. The first average delithiation capacities of SiO, SiO/C-40, SiO/C-80 and SiO/C-120 are 900, 1142, 1129 and 1050 mA h g⁻¹ at a current density of 1 A g⁻¹, respectively. It is worth noting that the capacity of SiO gradually increases during the initial 60 cycles. The pristine SiO film has a small specific surface area, which leads to poor electrolyte wetting during the early cycles, and its low plateau voltage on the lithiation curve in Fig. 5a is attributed to its poor intrinsic electronic conductivity. Therefore, the as-deposited SiO shows a low reversible capacity during the initial cycles. In the subsequent cycles, due to the volume effect of the active material, SiO film gradually cracks and the specific surface area increases, which is beneficial to the electrolyte wetting [37]. In this

experiment, the pristine SiO thin film anodes require 50–60 cycles to increase the specific surface area to achieve full activation at a large current density. The co-sputtered carbon plays a role of conductive additive, which enhances the conductive network inside the SiO film, hence the cycle numbers required to reach the maximum reversible capacity are decreased for SiO/C films (Fig. 5b). However, SiO/C-120 shows a lower capacity than the SiO, probably due to the steric hindrance of excessive carbon, which causes a larger electrochemical polarization, thus resulting in a decrease of the capacity [36]. After 500 cycles, the capacity retentions of as-deposited SiO/C thin films are 87.7% ± 1.0%, 87.3% ± 2.0%, 91.1% ± 1.0% and 88.2% ± 1.0%, respectively.

Since SiO/C-80 shows the best cycle performance among three carbonic samples, its rate capability has been further studied in Fig. 5c. It is observed that SiO has only 960 mA h g⁻¹ at 1 A g⁻¹ (compared with the maximum capacity of ~1200 mA h g⁻¹ in Fig. 5b) because the electrode is not able to be fully lithiated/delithiated due to its large polarization at a high current density. Moreover, the capacity of SiO/C-80 at 5 A g⁻¹ is 56.9% of that at 0.1 A g⁻¹, while SiO is only 45.1%. The above results indicate that SiO/C-80 shows a remarkable electrochemical reversibility at high current density.

Fig. 6a shows the further cycle performance of SiO and SiO/C-80. SiO/C-80 still shows a capacity retention of 82.0% ± 0.5% after 750 cycles while SiO shows 79.1% ± 2.0%. Fig. 6b shows the zoom-in for

Table 2
Electrochemical properties of SiO/C thin films.

Sample	Specific capacity (mA h g ⁻¹)		Initial coulombic efficiency (%)	Retention (%) / 500 cycles
	Delithiation	Lithiation		
SiO	1012	1775	57.0 ± 0.6	87.7 ± 1.0
SiO/C-40	1320	1811	72.8 ± 0.4	87.3 ± 2.0
SiO/C-80	1393	1940	72.0 ± 1.0	91.1 ± 1.0
SiO/C-120	1256	1886	66.5 ± 1.0	88.2 ± 1.0

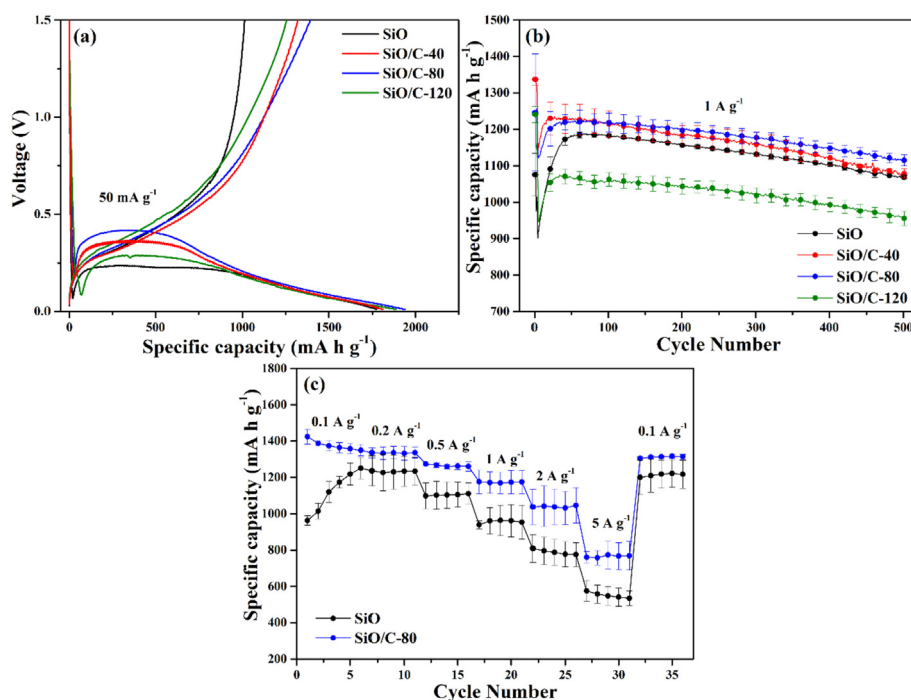


Fig. 5. (a) Lithiation–delithiation profiles of as-deposited thin films in the 1st cycle. Delithiation specific capacities vs. cycle number of as-deposited films at a current density of (b) 1 A g⁻¹, (c) 0.1–5 A g⁻¹.

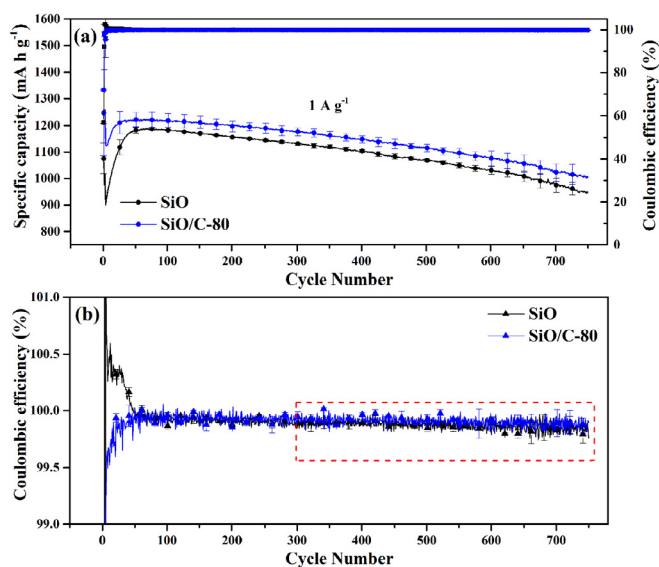


Fig. 6. Cycle performance of as-deposited SiO and SiO/C-80 (a) delithiation specific capacities and coulombic efficiency vs. cycle number at a current density of 1 A g^{-1} , (b) the zoom-in for the coulombic efficiency.

the coulombic efficiency of SiO and SiO/C-80. SiO shows an ICE of $\sim 57\%$ due to its poor intrinsic electronic conductivity. It has large polarization during the first cycle, and a part of lithium in the Li–Si alloy cannot be completely removed due to kinetic factors. In the subsequent cycles, due to the volume effect of the active material, the SiO film gradually cracks and the specific surface area increases. An extra part of lithium can be extracted during the initial tens of cycles (from the Li–Si alloy generated in the first cycle), so the coulombic efficiency in this stage is higher than 100%. When this part of lithium is completely extracted, the coulombic efficiency will be stabilized at around 99.8%.

The situation of SiO/C-80 is different. The co-sputtered carbon increases the electronic conductivity of the film and reduces the reaction polarization. The first lithiation–delithiation of SiO/C-80 goes through thoroughly. SiO/C-80 undergoes an activation process during the subsequent cycles, so it shows a coulombic efficiency of 98.6% in the second cycle and gradually increases to $\sim 99.9\%$. As shown in Fig. 6b, the average coulombic efficiency of SiO/C-80 after 300 cycles is significantly higher than SiO, which means a better cycle performance of SiO/C-80.

The above results clearly indicate that the co-sputtered carbon can improve the electrochemical performance of SiO film electrodes, and SiO/C-80 exhibits a remarkable cycle performance among as-deposited samples.

The CV curves of as-deposited SiO/C thin films are displayed in Fig. 7. The cathodic peak below 0.2 V corresponds to the formation of Li–Si alloy. It can be observed that SiO, SiO/C-40 and SiO/C-120 suffer a large polarization in the first lithiation process, and the cathodic peak current gradually increases but does not reach the maximum when the potential is scanned to 0.01 V (Fig. 7a, b, d). The peak current and peak area of SiO in the third cycle increase significantly compared to the second cycle, which is corresponded to the capacity rise-up process. The second and third CV curves of SiO/C-80 are basically coincident, and the anodic peak appears at 0.3 V compared to 0.5 V of SiO, indicating that SiO/C-80 has a small polarization in both lithiation and delithiation processes, and has admirable reversibility in the first several cycles (Fig. 7c).

3.3. Ex-situ SEM

The effects of the co-sputtered carbon on the surface morphology and structure of the as-deposited SiO thin film anode during cycling have been investigated by ex-situ SEM analysis (Fig. 8). After the first cycle, only a few cracks have generated in a part of the SiO surface, while SiO/C-80 has been broken into islands with tens of microns in size (Fig. 8a and e). These islands enlarge the specific surface area of the thin film anode, which is beneficial

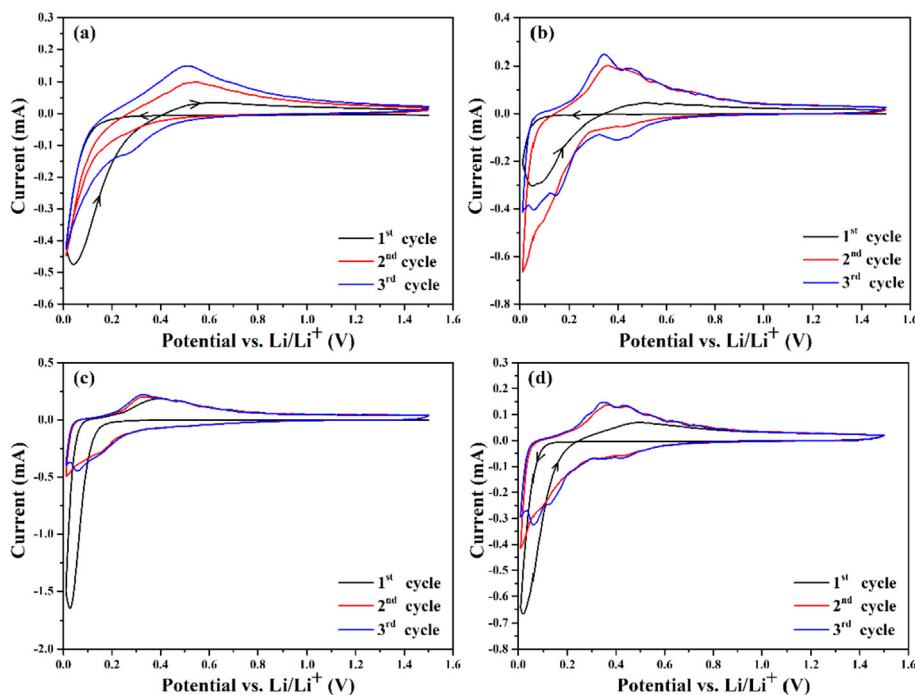


Fig. 7. CV curves of as-deposited (a) SiO, (b) SiO/C-40, (c) SiO/C-80, (d) SiO/C-120.

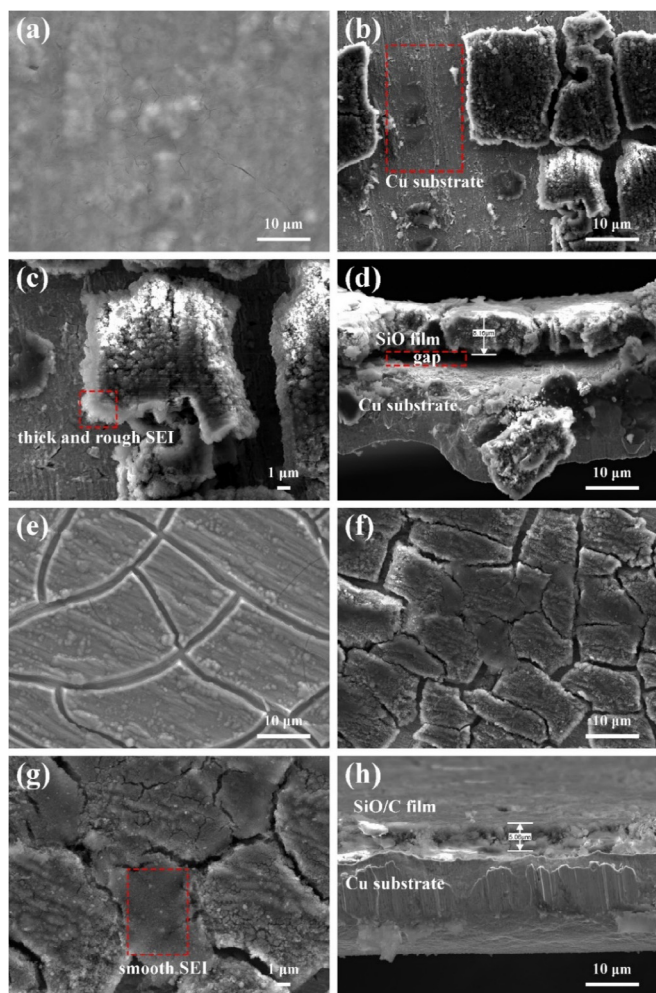


Fig. 8. SEM images of as-deposited SiO after (a) the 1st cycle, (b) the 500th cycle, (c) higher magnification of (b), (d) cross section after the 500th cycle, and SiO/C-80 after (e) the 1st cycle, (f) the 500th cycle, (g) higher magnification of (f), (h) cross section after the 500th cycle.

to the electrolyte wetting, and results in higher capacity during the initial cycles (Fig. 5b). Previous study has proved that the cracking

at the beginning of the cycle will enhance the contact of the SiO_x surface with the electrolyte, and will shorten the lithium ion diffusion path, which is beneficial to the Li-capacity of the electrode [37]. Soni et al. have proposed a shear lag model [38], namely, the smaller size the silicon-island has, the larger proportion the shear lag area occupies. The shear lag area does not undergo plastic deformation during lithiation-delithiation processes, which is beneficial to maintain structural stability. During cycling process, the cracks on the electrode surface gradually increase, which induces the pulverization of the active materials and the destruction of the conductive network, resulting in a gradual capacity fading [37]. The poor electronic conductivity causes non-uniform distribution of current and stress inside SiO film during cycling, which leads to a large plastic deformation and serious volume expansion. The thickness of SiO increases to 8.1 μm after 500 cycles, and an obvious delamination is found between the film and the Cu substrate (Fig. 8b and d). Similar to silicon thin film, the volume effect of SiO during the lithiation-delithiation processes leads to the formation of cracks, the electrode structure is destroyed, and the film will be peeled off from the current collector, causing a capacity fading with cycling [39]. Furthermore, the reduplicative volume effects cause fresh SiO surface to react with electrolyte, thus generate a thick and rough SEI layer at the debris edge (Fig. 8c). Lee et al. have synthesized Si/C co-sputtered thin film, where the carbon acts as a volume buffer, which reduces the stresses caused by volume expansion during cycling [40]. The co-sputtered carbon in SiO/C film helps to maintain the integrity of the islands, and its excellent conductivity homogenizes the current and stress inside the film during further cycling [41], so that no obvious pulverization and delamination are observed in SiO/C-80 (Fig. 8f and g). The thickness of SiO/C-80 is 5.0 μm after 500 cycles (Fig. 8h), which corresponds to the good cycle performance in Fig. 5b. In summary, the co-sputtered carbon not only increases the conductivity inside the film, which makes a larger specific surface area and capacity in the first cycle, but also alleviates the in-plane stress during cycling and maintains the electrode structure, resulting in an improved cycle performance. The mechanism of the co-sputtered carbon during cycling is shown in Fig. 9.

3.4. Electrochemical impedance spectroscopy and Li-ion diffusion

To better understand the effect of co-sputtered carbon on the lithiation/delithiation kinetics of as-deposited SiO/C films, EIS

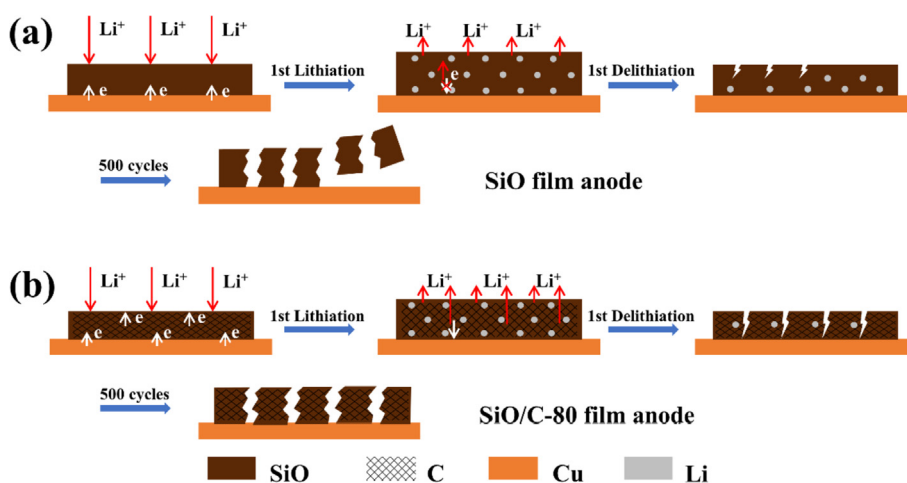


Fig. 9. Schematic illustration of the mechanism of SiO/C film for improving the electrochemical performance.

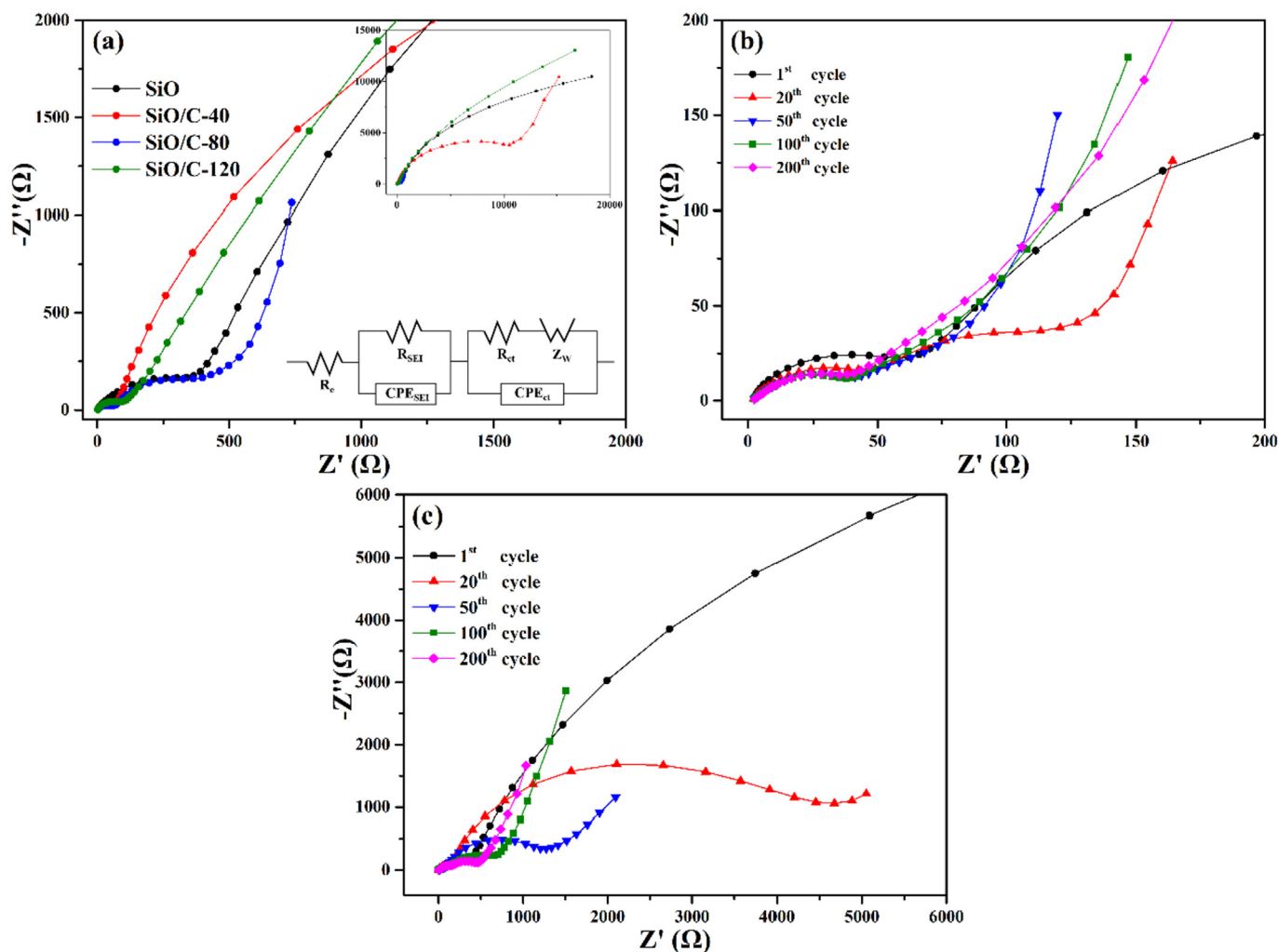


Fig. 10. (a) Nyquist plots of SiO and SiO/C films after the 1st cycle and the equivalent circuit model, (b) Nyquist plots of SiO/C-80 after different cycles, (c) Nyquist plots of SiO after different cycles.

measurements have been studied at delithiated state after different cycles, as shown in Fig. 10. The Nyquist plots consist of two semicircles at high frequency and medium frequency region and a slope at low frequency region, and the inset of Fig. 10a is the equivalent circuit used for modeling the impedance spectra. The diameter of the semicircle at high frequency region represents the SEI film resistance (R_{SEI}), the diameter of the semicircle at medium frequency region represents the charge transfer resistance (R_{ct}) between electrode and electrolyte interphase, and the slope at low frequency region is assigned to the Warburg impedance (Z_w), which is associated with Li-ion diffusion inside the SiO/C film [23]. The R_{ct} of SiO/C-80 is determined to be 226Ω after the first cycle, which is far below than the other three samples (inset of Fig. 10a). The Nyquist plots of SiO/C-80 after different cycles are shown in Fig. 10b, the R_{ct} of SiO/C-80 after 20, 50, 100, 200 cycles are 52, 43, 33, and 26Ω , respectively, which are significantly lower than those of SiO (Fig. 10c). The two semicircles overlap after 50 cycles, and the R_{ct} decreases with cycling, which are associated to the continuous capacity rise-up process during early cycles (Fig. 5b). These results suggest that SiO/C-80 has a lower R_{ct} value during cycling, which enables higher exchange current densities ($i_0 = RT/nFR_{ct}$), thus exhibits a remarkable rate capability [42].

In order to further study the effect of co-sputtered carbon on the Li-ion diffusion in SiO film, we have determined the lithium-ion

chemical diffusion coefficients ($D_{Li^+}^+$) of the as-deposited SiO/C films by using EIS method [43,44]. Fig. 11a gives the Nyquist plots of the as-deposited SiO/C films delithiated at 50% state of charge (SOC) at 55°C after the first cycle, since the high temperature is beneficial to the lithiation/delithiation reaction kinetics during the initial cycles [43]. The Warburg diffusion occurred over a frequency range of around 1–0.1 Hz at 55°C , and the linear dependence of Z' on $\omega^{-1/2}$ are observed in Fig. 11b. The slope of the fitting line is known as Warburg factor A_w . The $D_{Li^+}^+$ values can be calculated according to the following equation [43,45]:

$$D_{Li^+} = 0.5 \left(\frac{RT}{F^2 n^2 S A_w C} \right)^2$$

where R ($\text{J mol}^{-1} \text{K}^{-1}$) is the gas constant, T (K) is the absolute temperature, n is the extraction number per molecule during delithiation, F (C mol^{-1}) is the Faraday constant, S (cm^2) is the surface area of the SiO/C thin film anode, C (mol cm^{-3}) is the volumetric molar concentration of the inserted Li-ions and A_w ($\Omega \text{Hz}^{1/2}$) is the Warburg factor. The $D_{Li^+}^+$ values of SiO, SiO/C-40, SiO/C-80, SiO/C-120 are 3.17×10^{-13} , 3.67×10^{-13} , 3.95×10^{-13} , and $2.57 \times 10^{-13} \text{ cm}^2 \text{s}^{-1}$ at 50% SOC after the first cycle, respectively. The lower capacity of SiO in Fig. 5b during early cycles is attributed to its low $D_{Li^+}^+$ value. With the carbon co-sputtering, the electronic

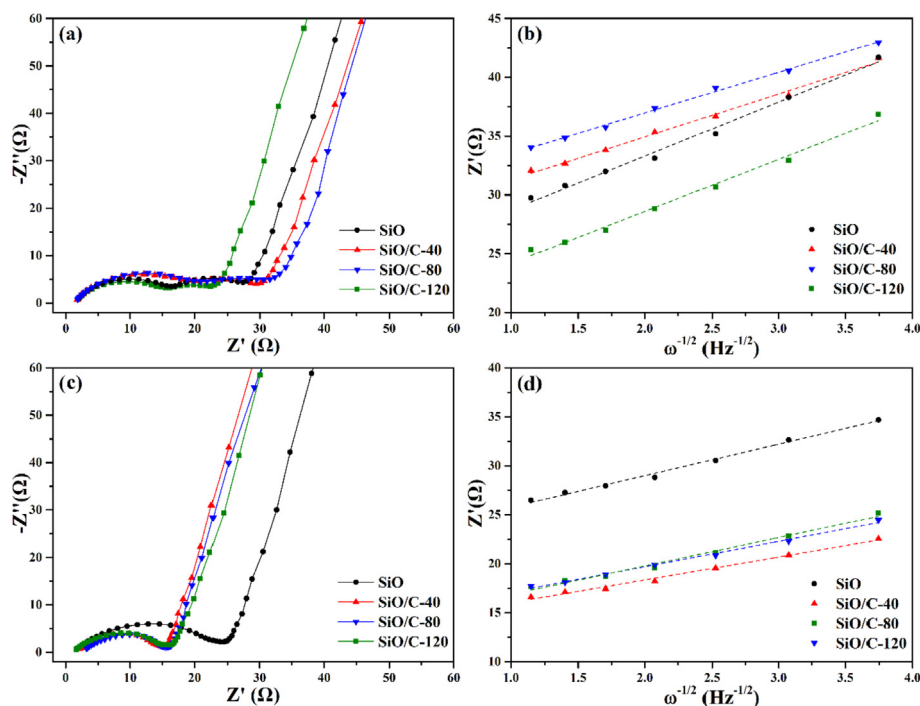


Fig. 11. (a) Nyquist plots of SiO and SiO/C films at 50% SOC at 55 °C after the 1st cycle, (b) Z' vs $\omega^{-1/2}$ and the linear fitting, (c) Nyquist plots of SiO and SiO/C films at 50% SOC at 55 °C after the 100th cycle, (d) Z' vs $\omega^{-1/2}$ and the linear fitting.

conductivity of the film is enhanced. SiO/C film cracks into islands, which shortens the diffusion paths of Li^+ , thus the D_{Li^+} values of SiO/C-80 and SiO/C-40 are higher than the SiO. However, the excessive carbon in SiO/C-120 has a steric hindrance to lithium ion diffusion although it enhances the conductive network inside the film, which leads to a lower D_{Li^+} value than SiO.

After 100 cycles, the capacities of the as-deposited thin films reach to the maximum since the electrodes have been fully cracked into islands. The lithium-ion diffusion paths are shortened, which makes a decrease in the R_{ct} values (Fig. 11c). The D_{Li^+} values increase to 6.49×10^{-13} , 7.35×10^{-13} , 8.66×10^{-13} , and $6.01 \times 10^{-13} \text{ cm}^2 \text{ s}^{-1}$ at 50% SOC, respectively. The D_{Li^+} values of the as-deposited samples increase significantly, however the D_{Li^+} value of SiO/C-120 is still lower than SiO due to the excessive carbon inside the film. These results have evidenced that a moderate amount of carbon increases the surface area as well as the electrolyte wetting of the electrode, thus indirectly improves the lithium-ion diffusion in SiO film, whereas an excessive amount of carbon has a negative effect on the lithium-ion diffusion.

4. Conclusions

SiO/C thin film anodes with different carbon contents have been prepared on Cu foils by magnetron co-sputtering method. Obviously positive effects on ICE and cycle stability have been observed with the carbon addition. SiO/C-80 with a thickness of 1.15 μm shows a remarkable performance in terms of ICE, reversible capacity, cycling stability and rate capability. A moderate amount of co-sputtered carbon enhances the electronic conductivity inside the film, which results in a larger surface area and higher delithiation capacity after the first cycle. On the other hand, the uniformly distributed carbon enables the electrode to homogenize the current and internal stress during cycling, so that the volume expansion is alleviated, and the physical structure can be maintained after long-term cycle. These results suggest that the co-

sputtered carbon is significant for improving the electrochemical performance of the SiO thin film anodes. Importantly, these thin film anodes prepared by facile sputtering method have potential applications in all-solid-state batteries.

Conflicts of interest

The authors declare no conflict of interest.

Acknowledgements

This work is supported by the National Key Research and Development Program of China (No. 2017YFB0102000), and the National Natural Science Foundation of China (51777208, 21621091). The authors also thank Prof. D. W. Liao for his valuable suggestions.

References

- [1] A. Patil, V. Patil, D. Wook Shin, J.-W. Choi, D.-S. Paik, S.-J. Yoon, Issue and challenges facing rechargeable thin film lithium batteries, *Mater. Res. Bull.* 43 (2008) 1913–1942.
- [2] C. Sun, J. Liu, Y. Gong, D.P. Wilkinson, J. Zhang, Recent advances in all-solid-state rechargeable lithium batteries, *Nano Energy* 33 (2017) 363–386.
- [3] X. Yao, D. Liu, C. Wang, P. Long, G. Peng, Y.-S. Hu, H. Li, L. Chen, X. Xu, High-energy all-solid-state lithium batteries with ultralong cycle life, *Nano Lett.* 16 (2016) 7148–7154.
- [4] F.L. Cras, B. Pecquenard, V. Dubois, V.P. Phan, D. Guy-Bouysson, All-solid-state lithium-ion microbatteries using silicon nanofilm anodes: high performance and memory effect, *Adv. Energy Mater.* 5 (2015), 1501061.
- [5] J.R. Szczech, S. Jin, Nanostructured silicon for high capacity lithium battery anodes, *Energy Environ. Sci.* 4 (2011) 56–72.
- [6] Q. Sa, Y. Wang, Ni foam as the current collector for high capacity C–Si composite electrode, *J. Power Sources* 208 (2012) 46–51.
- [7] U. Kasavajjula, C. Wang, A.J. Appleby, Nano- and bulk-silicon-based insertion anodes for lithium-ion secondary cells, *J. Power Sources* 163 (2007) 1003–1039.
- [8] H. Li, X. Huang, L. Chen, G. Zhou, Z. Zhang, D. Yu, Y.J. Mo, N. Pei, The crystal structural evolution of nano-Si anode caused by lithium insertion and extraction at room temperature, *Solid State Ionics* 135 (2000) 181–191.

- [9] F. Holtstiege, A. Wilken, M. Winter, T. Placke, Running out of lithium? A route to differentiate between capacity losses and active lithium losses in lithium-ion batteries, *Phys. Chem. Chem. Phys.* 19 (2017) 25905–25918.
- [10] A.J. Smith, J.C. Burns, D. Xiong, J.R. Dahn, Interpreting high precision coulometry results on Li-ion cells, *J. Electrochem. Soc.* 158 (2011) A1136–A1142.
- [11] J. Maranchi, A. Hepp, P. Kumta, High capacity, reversible silicon thin-film anodes for lithium-ion batteries, *Electrochem. Solid State Lett.* 6 (2003) A198–A201.
- [12] N. Wang, T. Hang, W. Zhang, M. Li, Highly conductive Cu nanoneedle-array supported silicon film for high-performance lithium ion battery anodes, *J. Electrochem. Soc.* 163 (2016) A380–A384.
- [13] L. Chen, J. Xie, H. Yu, T. Wang, Si-Al thin film anode material with superior cycle performance and rate capability for lithium ion batteries, *Electrochim. Acta* 53 (2008) 8149–8153.
- [14] A. Reyes Jiménez, R. Klöpsch, R. Wagner, U.C. Rodehorst, M. Kolek, R. Nölle, M. Winter, T. Placke, A step toward high-energy silicon-based thin film lithium ion batteries, *ACS Nano* 11 (2017) 4731–4744.
- [15] Y.H. Jouybari, F. Berkemeier, Enhancing silicon performance via LiPON coating: a prospective anode for lithium ion batteries, *Electrochim. Acta* 217 (2016) 171–180.
- [16] A.R. Jiménez, R. Nölle, R. Wagner, J. Hüsker, M. Kolek, R. Schmich, M. Winter, T. Placke, A step towards understanding the beneficial influence of a LiPON-based artificial SEI on silicon thin film anodes in lithium-ion batteries, *Nanoscale* 10 (2018) 2128–2137.
- [17] Y. Tong, Z. Xu, C. Liu, G.a. Zhang, J. Wang, Z.G. Wu, Magnetic sputtered amorphous Si/C multilayer thin films as anode materials for lithium ion batteries, *J. Power Sources* 247 (2014) 78–83.
- [18] S.C. Jung, H.-J. Kim, J.-H. Kim, Y.-K. Han, Atomic-level understanding toward a high-capacity and high-power silicon oxide (SiO) material, *J. Phys. Chem. C* 120 (2015) 886–892.
- [19] T. Chen, J. Wu, Q. Zhang, X. Su, Recent advancement of SiO_x based anodes for lithium-ion batteries, *J. Power Sources* 363 (2017) 126–144.
- [20] R. Miyazaki, N. Ohta, T. Ohnishi, K. Takada, Anode properties of silicon-rich amorphous silicon suboxide films in all-solid-state lithium batteries, *J. Power Sources* 329 (2016) 41–49.
- [21] W.L. Zhang, S. Zhang, M. Yang, T.P. Chen, Microstructure of magnetron sputtered amorphous SiO_x films: formation of amorphous Si core-shell nanoclusters, *J. Phys. Chem. C* 114 (2010) 2414–2420.
- [22] A. Hohl, T. Wieder, P. Van Aken, T. Weirich, G. Denninger, M. Vidal, S. Oswald, C. Deneke, J. Mayer, H. Fuess, An interface clusters mixture model for the structure of amorphous silicon monoxide (SiO), *J. Non-Cryst. Solids* 320 (2003) 255–280.
- [23] Y. Yamada, Y. Iriyama, T. Abe, Z. Ogumi, Kinetics of electrochemical insertion and extraction of lithium ion at SiO, *J. Electrochem. Soc.* 157 (2010) A26–A30.
- [24] T. Kim, S. Park, S.M. Oh, Solid-state NMR and electrochemical dilatometry study on Li⁺ uptake/extraction mechanism in SiO electrode, *J. Electrochem. Soc.* 154 (2007) A1112–A1117.
- [25] C.-M. Park, W. Choi, Y. Hwa, J.-H. Kim, G. Jeong, H.-J. Sohn, Characterizations and electrochemical behaviors of disproportionated SiO and its composite for rechargeable Li-ion batteries, *J. Mater. Chem.* 20 (2010) 4854–4860.
- [26] X. Meng, H. Huo, Z. Cui, X. Guo, S. Dong, Influences of oxygen content on the electrochemical performance of a-SiO_x thin-film anodes, *Electrochim. Acta* 283 (2018) 183–189.
- [27] H. Takezawa, K. Iwamoto, S. Ito, H. Yoshizawa, Electrochemical behaviors of nonstoichiometric silicon suboxides (SiO_x) film prepared by reactive evaporation for lithium rechargeable batteries, *J. Power Sources* 244 (2013) 149–157.
- [28] Q. Si, K. Hanai, T. Ichikawa, M. Phillipps, A. Hirano, N. Imanishi, O. Yamamoto, Y. Takeda, Improvement of cyclic behavior of a ball-milled SiO and carbon nanofiber composite anode for lithium-ion batteries, *J. Power Sources* 196 (2011) 9774–9779.
- [29] A. Guerfi, P. Charest, M. Dontigny, J. Trottier, M. Lagace, P. Hovington, A. Vijn, K. Zaghbi, SiO_x-graphite as negative for high energy Li-ion batteries, *J. Power Sources* 196 (2011) 5667–5673.
- [30] M. Yamada, A. Ueda, K. Matsumoto, T. Ohzuku, Silicon-based negative electrode for high-capacity lithium-ion batteries: “SiO”-carbon composite, *J. Electrochem. Soc.* 158 (2011) A417–A421.
- [31] T. Hatchard, J. Dahn, In situ XRD and electrochemical study of the reaction of lithium with amorphous silicon, *J. Electrochem. Soc.* 151 (2004) A838–A842.
- [32] R. Alfonsetti, L. Lozzi, M. Passacantando, P. Picozzi, S. Santucci, XPS studies on SiO_x thin films, *Appl. Surf. Sci.* 70 (1993) 222–225.
- [33] C. Chandra, J. Kim, Silicon oxycarbide produced from silicone oil for high-performance anode material in sodium ion batteries, *Chem. Eng. J.* 338 (2018) 126–136.
- [34] T. Miyuki, Y. Okuyama, T. Kojima, T. Sakai, In-situ measurement of electrode thickness change during charge and discharge of a large capacity SiO anode, *Electrochemistry* 80 (2012) 405–408.
- [35] J.H. Ryu, J.W. Kim, Y.-E. Sung, S.M. Oh, Failure modes of silicon powder negative electrode in lithium secondary batteries, *Electrochem. Solid State Lett.* 7 (2004) A306–A309.
- [36] W. Wei, W. Lv, M.-B. Wu, F.-Y. Su, Y.-B. He, B. Li, F. Kang, Q.-H. Yang, The effect of graphene wrapping on the performance of LiFePO₄ for a lithium ion battery, *Carbon* 57 (2013) 530–533.
- [37] I. Choi, M.J. Lee, S.M. Oh, J.J. Kim, Fading mechanisms of carbon-coated and disproportionated Si/SiO_x negative electrode (Si/SiO_x/C) in Li-ion secondary batteries: dynamics and component analysis by TEM, *Electrochim. Acta* 85 (2012) 369–376.
- [38] S.K. Soni, B.W. Sheldon, X. Xiao, M.W. Verbrugge, A. Dongjoon, H. Haftbaradaran, G. Huajian, Stress mitigation during the lithiation of patterned amorphous Si islands, *J. Electrochem. Soc.* 159 (2011) A38–A43.
- [39] Y. He, X. Yu, Y. Wang, H. Li, X. Huang, Alumina-coated patterned amorphous silicon as the anode for a lithium-ion battery with high coulombic efficiency, *Adv. Mater.* 23 (2011) 4938–4941.
- [40] K.S. Lee, Y.N. Lee, Y.S. Yoon, Effect of carbon content on nanocomposite Si_{(1-x)C_x} thin film anode for all-solid-state battery, *Electrochim. Acta* 147 (2014) 232–240.
- [41] M.K. Jangid, F.J. Sonia, R. Kali, B. Ananthoju, A. Mukhopadhyay, Insights into the effects of multi-layered graphene as buffer/interlayer for a-Si during lithiation/delithiation, *Carbon* 111 (2017) 602–616.
- [42] P. Guo, H. Song, X. Chen, Electrochemical performance of graphene nano-sheets as anode material for lithium-ion batteries, *Electrochem. Commun.* 11 (2009) 1320–1324.
- [43] T. Zhang, H. Zhang, L. Yang, B. Wang, Y. Wu, T. Takamura, The structural evolution and lithiation behavior of vacuum-deposited Si film with high reversible capacity, *Electrochim. Acta* 53 (2008) 5660–5664.
- [44] J. Xie, N. Imanishi, T. Zhang, A. Hirano, Y. Takeda, O. Yamamoto, Li-ion diffusion in amorphous Si films prepared by RF magnetron sputtering: a comparison of using liquid and polymer electrolytes, *Mater. Chem. Phys.* 120 (2010) 421–425.
- [45] C. Ho, I. Raistrick, R. Huggins, Application of A-C techniques to the study of lithium diffusion in tungsten trioxide thin films, *J. Electrochem. Soc.* 127 (1980) 343–350.